Article:
Yu, Z, Jaworski, AJ and Backhaus, S (2010) A low-cost electricity generator for rural areas using a travelling-wave looped-tube thermoacoustic engine. Proceedings of the Institution of Mechanical Engineers, Part A: Journal of Power and Energy, 224 (6). 787 - 795. ISSN 0957-6509

https://doi.org/10.1243/09576509JPE864

A Low-Cost Electricity Generator for Rural Areas Using a Travelling-Wave Looped-Tube Thermoacoustic Engine

Zhibin Yu [1], Artur J Jaworski [1,*] and Scott Backhaus [2]

[1] School of Mechanical, Aerospace and Civil Engineering, University of Manchester, Sackville Street, PO Box 88, Manchester M60 1QD, United Kingdom

[2] Condensed Matter and Thermal Physics Group, Los Alamos National Laboratory, Los Alamos, NM 87545, United States

ABSTRACT

This article describes the construction and preliminary testing of a pre-prototype thermoacoustic electricity generator to test the concept of a low-cost device for application in remote or rural areas of developing countries. A travelling-wave thermoacoustic engine with a configuration of a looped-tube resonator is designed and constructed to convert heat to acoustic power. Air at atmospheric pressure is used as the working gas, PVC tubing is utilised for the feedback pipe, while an inexpensive commercially available loudspeaker is adopted to convert the acoustic power, produced by the engine, to electricity. Preliminary experimental results are presented and discussed in detail. The results show that the approach is feasible in principle and it is possible to produce the electrical power levels in the order of 4-5 W with overall heat-to-electric efficiencies in the order of 1%. Further work towards optimising the device from the performance, manufacturing and cost point of view is outlined.

1. Introduction and background

Thermoacoustic engines have attracted a lot of attention [1,2] because their only moving component is the gas undergoing the acoustic motion. The absence of mechanical moving parts provides a potential for high reliability and low cost. The working gas in thermoacoustic engines is usually a noble gas, making this technology environmentally friendly. Furthermore, the required operating temperature difference could be relatively small. For example, de Blok's [3] travelling-wave engine starts the acoustic oscillation at a temperature difference of only 65 K. Therefore the technology shows a lot of potential for utilizing solar power and waste heat. On the other hand, in the past decades, a variety of thermoacoustic engines, either standing-wave or travelling-wave thermoacoustic engines, have been designed and tested. One of the remaining challenges is to improve the thermal efficiency. So far, the highest thermal efficiency (defined as a ratio of acoustic power delivered to the quarter wavelength resonator over the heat input) reached 30% in a travelling-wave thermoacoustic engine using high pressure helium to execute a Stirling-like thermodynamic cycle in a carefully designed acoustic network [2]. This corresponds to 41% of the Carnot efficiency.

The acoustic power of the thermoacoustic engine derived from the heat input can be utilized in several ways for different applications. It is generally used for two main purposes: One is to drive coolers or heat pumps [4], which can

* Corresponding author; E-mail: a.jaworski@manchester.ac.uk; Tel: +44(0)161-275-4352

be either thermoacoustic coolers (heat pumps) or pulsed-tube coolers. The other is to directly convert the acoustic power to electricity through the electro-dynamic transduction mechanism. Usually, flexure-bearing-supported linear alternators are an excellent solution due to their high reliability and efficiency. For example for the travelling-wave thermoacoustic electric generator developed by Backhaus *et al.* [5] the maximum system efficiency (defined as the electric power output over heat input) reached 18%, whilst the alternator efficiency (defined as the electric power output over acoustic power absorbed by the alternator) reached 75%, while the engine efficiency (defined as acoustic power absorbed by the alternator over the heat input) reached 24%, which corresponds to 35.7% of the Carnot efficiency.

However, linear alternators purpose-designed for thermoacoustic applications are costly – in the order of a few thousands of US dollars. This limits the advantages of the thermoacoustic heat engines for low-cost energy conversion devices understood here as being in the range of a few tens of US dollars for electrical power outputs in the order of a hundred Watts. Usually, ordinary audio loudspeakers are excluded as prospective candidates for linear alternators due to their relatively low power transduction efficiency, a fragile cone, and a limited stroke, especially when the researchers aim at obtaining generators with a high power, high efficiency and high pressure difference between the two sides of the diaphragm. However, it is possible to consider niche applications where the main driver is the cost of device, not the power transduction (or even the overall) efficiency. This is particularly true for the above mentioned waste heat and solar energy utilization applications, where a low grade thermal energy is abundant and could be considered a limitless source. Then the actual efficiency figures may become a secondary issue, as long as the electric power could be extracted at very low cost per kWh_e. Similar reasoning may be true for designing cheap electricity generators for developing countries [6]. The current work is part of a collaborative project, with an acronym SCORE, funded through the Engineering and Physical Sciences Research Council UK [7], and attempts to explore the possibilities of using commercially available loudspeakers (or their re-engineered parts) to develop cheap thermoacoustic electricity generators driven by biomass combustion. This preliminary study attempts to develop a laboratory-based demonstration (pre-prototype) concept. The aim of the demonstrator is to produce a few Watts of electricity from a setup that could be potentially streamlined towards a low-cost design. It is hoped that the final scaled-up version ready for commercialisation will be able to produce up to 150W of electricity, will cost around 30 US dollars when all the components are designed for mass production and assembly, and will be ready for implementation through appropriate charities working with rural communities around the world.

2. Theoretical analysis of an alternator

In the analysis presented below it is assumed that an alternator has a linear behaviour and that the hysteresis losses can be ignored. In this case, a simple linear model can be formulated [8,9] that describes the use of a loudspeaker as a linear alternator, as shown schematically in Figure 1. The acoustic wave exerts an oscillatory pressure on the diaphragm, which has an effective area S. The total mass of the diaphragm and the coil is M_m. The alternator has a mechanical stiffness, K_m, and a mechanical resistance, R_m. The coil has an inductance, L_e, and a resistance, R_e. The force factor is Bl. A load resistor R_L is connected to the terminals of the coil to extract the electrical power converted from the acoustic power by the alternator. The sketch at the bottom of Figure 1 shows the equivalent impedance circuit of the physical model shown at the top. The pressure difference (pressure drop) between the front and the back of the diaphragm is Δp, the volumetric velocity due to the diaphragm displacement is U_1. The force exerted on the diaphragm due to the pressure drop is F, and velocity of the diaphragm is u_1. The voltage on the load resistor is V_L, and the current is I_1.

The model in Figure 1 can be described approximately by the following linear equations:

$$\Delta p = \frac{BlI_1}{S} + \frac{R_m + j\left(\omega M_m - \frac{K_m}{\omega}\right)}{S^2} U_1 \tag{1}$$

$$\frac{BlU_1}{S} = \left(R_e + R_L + j\omega L_e\right) I_1 \tag{2}$$

The input acoustic power P_a is defined as

$$P_a = \frac{1}{2}\mathrm{Re}\left[\Delta p \tilde{U}_1\right] = \frac{1}{2}\left|\Delta p\right|\left|U_1\right|\cos(\theta). \tag{3}$$

In equation (3), θ is the phase angle between the pressure drop and velocity. The extracted electric power by the load resistor, P_e is defined as

$$P_e = \frac{1}{2} R_L \left|I_1\right|^2 = \frac{1}{2}\frac{\left|V_L\right|^2}{R_L}. \tag{4}$$

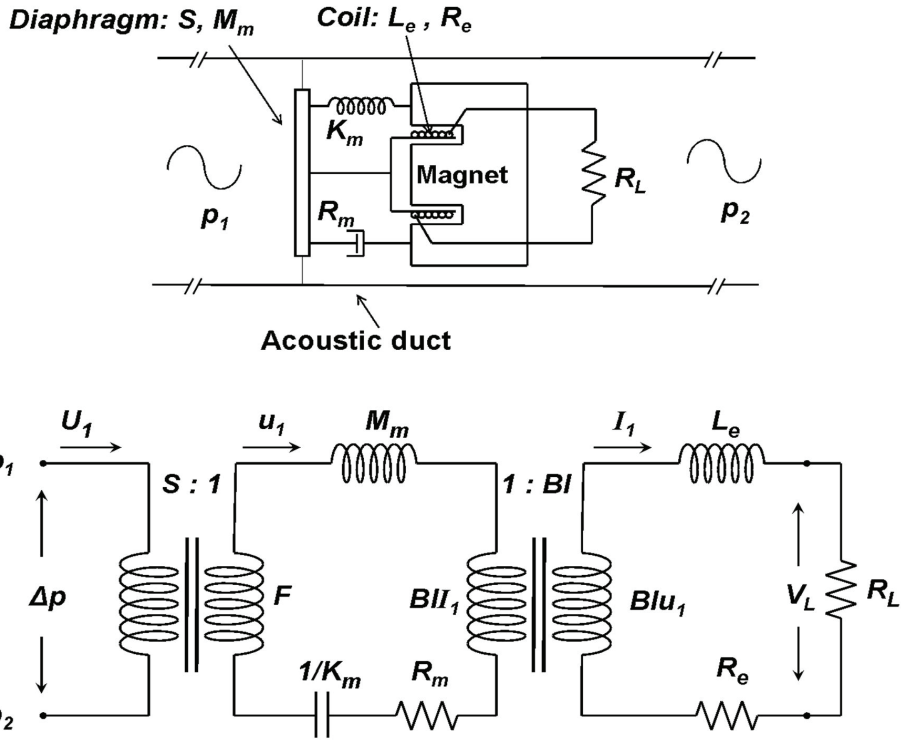

Figure 1 Schematic of the physical model of the alternator (top); the equivalent impedance circuit (bottom).

In equation (4), $|V_L|$ is the amplitude of current V_L. Accordingly, the acoustic-electric efficiency can be defined as

$$\eta_{A-E} = \frac{P_e}{P_a}. \tag{5}$$

Substituting Equations (1) and (2) into equation (3) leads to the following relationship:

$$P_a = \frac{1}{2}\mathrm{Re}\left[\Delta p \tilde{U}_1\right] = \frac{1}{2}\frac{|U_1|^2}{S^2}\left[R_m + \frac{(Bl)^2 R_e}{(R_e+R_L)^2+\omega^2 L_e^2} + \frac{(Bl)^2 R_L}{(R_e+R_L)^2+\omega^2 L_e^2}\right] \quad (6)$$

From Equation (6), it can be found that the input acoustic power, P_a, is dissipated by the alternator by three different mechanisms: the mechanical resistance, the resistance of the coil and the load resistor. According to Equation (6) and neglecting the inductance of the coil, the electrical power extracted by the load resistor can be written as:

$$P_e = \frac{1}{2}\frac{|U_1|^2}{S^2}\frac{(Bl)^2 R_L}{(R_e+R_L)^2}. \quad (7)$$

The maximum power extracted is therefore

$$P_{e,\max} = \frac{1}{8}\frac{|U_1|^2}{S^2}\frac{(Bl)^2}{R_e} \quad (8)$$

when

$$R_L = R_e \quad (9)$$

For the loudspeaker tested in this work, ωL_e is much lower than R_e or R_L. Therefore, substituting Equations (6) and (7) into (5) and neglecting the inductance of the coil, the approximate expression for the efficiency can be obtained as

$$\eta_{A-E} = \frac{(Bl)^2 R_L}{R_m(R_e+R_L)^2 + (Bl)^2(R_e+R_L)} \quad (10)$$

The maximum efficiency can be obtained as

$$\eta_{A-E,\max} = \frac{(Bl)^2\sqrt{1+\frac{(Bl)^2}{R_m R_e}}}{R_m R_e\left(1+\sqrt{1+\frac{(Bl)^2}{R_m R_e}}\right)^2 + (Bl)^2\left(1+\sqrt{1+\frac{(Bl)^2}{R_m R_e}}\right)} \quad (11)$$

when

$$R_L = R_e\sqrt{1+\frac{(Bl)^2}{R_m R_e}} \quad (12)$$

Substituting equation (2) into (1) to cancel I_1 leads to the total acoustic impedance of the alternator:

$$Z_{total} = \frac{\Delta p}{U_1} = \frac{1}{S^2}\left[\frac{(Bl)^2}{(R_e+R_L+j\omega L_e)} + R_m + j\left(\omega M_m - \frac{K_m}{\omega}\right)\right]. \quad (13)$$

The inductance of the coil can be neglected, because ωL_e is much lower than R_e or R_L. Then the phase angle between pressure drop, Δp, and the volumetric velocity, U_1, can be derived from equation (13) as

$$\theta = \text{atan}\left[\frac{\omega M_m - \frac{K_m}{\omega}}{\frac{(Bl)^2}{(R_e + R_L)} + R_m}\right]. \quad (14)$$

In Equation (14), when $\omega^2 = M_m K_m$, i.e. the alternator is at resonance, the phase angle between Δp and U_1 is

$$\theta = 0 \text{ , or } \theta = \pm\pi \text{ .} \quad (15)$$

Therefore, by monitoring the phase angle θ, one can find out whether the alternator is at resonance. However, it should be noted that the analysis is based on the ideal linear conditions. In a practical linear alternator, the mechanical resistance depends on frequency, because the mechanical windage and spring losses depend on the frequency. Furthermore, at high pressure amplitudes, the harmonics will also be induced in the engine.

3. Experimental setup

The experimental setup is shown schematically in Figure 2. The main cold heat exchanger is made out of a round aluminium block, which is 90 mm in length, and 110 mm in diameter. Gas passages are made in the form of 45 holes with the diameter of 5 mm, drilled parallel to the centre-line of the heat exchanger. 12 holes with the diameter of 6 mm are drilled perpendicular to the heat exchanger axis to pass cooling water A PCB pressure transducer (model 112A22) is installed on the flange just above the cold heat exchanger (denoted as P3 in Figure 2).

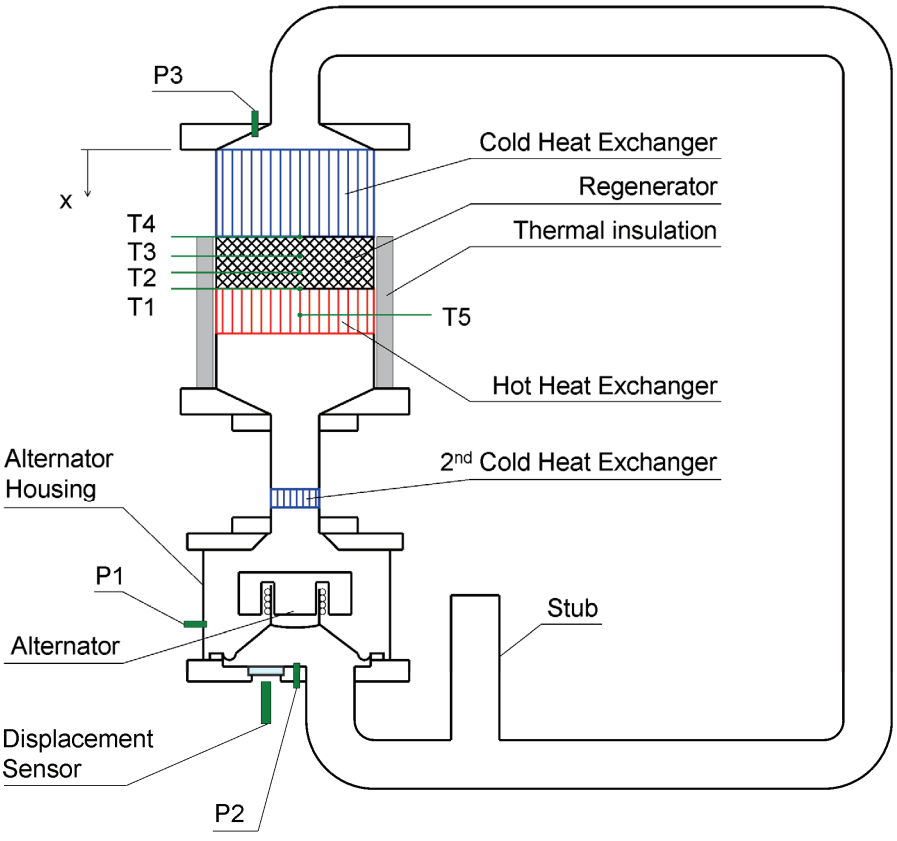

Figure 2 Schematic diagram of the test rig.

The regenerator is made out of stainless screen disks (110 mm in diameter), with the mesh number 34 and the wire diameter 0.254 mm. Sixty six discs have been piled up in a stainless steel can which has a wall thickness of 2 mm. The disks form a 33 mm long regenerator. Consequently, the calculated porosity and hydraulic radius are 73.3% and 175 μm, respectively. Four Type-K thermocouples (TC-Direct model 408-119) are embedded in the regenerator. The distance between each of the two adjacent thermocouples is 11 mm. They monitor the temperature profile along the axis of the regenerator, as well as the temperature difference between the two ends of the regenerator. They are denoted as T1 – T4.

The hot heat exchanger is made in a similar way to the cold heat exchanger, except that it is made out of brass to withstand much higher temperatures (brass melting temperature is typically around 900-940°C, while the expected hot heat exchanger temperatures were up to 650°C). It is also 110 mm in diameter, but only 51 mm in length. There are 64 holes of 7 mm diameter, parallel to the axis for passing working gas. Perpendicular to the axis, 9 quarter-inch holes have been drilled to hold nine cartridge heaters. Each cartridge heater can provide 100 W of heat input. As a result, the input thermal power can be varied between 100 and 900 W with a step of 100 W. Thermocouple T5 penetrates 55 mm into the brass block to monitor the metal temperature at the centre of the hot heat exchanger.

Below the hot heat exchanger, there is a short thermal buffer tube, which is simply a section of stainless steel pipe (ID=110 mm) with a length of 55 mm, and a wall thickness of 2 mm. The four parts described so far are clamped between two 4 inch flanges as shown in Figure 2. To reduce heat losses, the regenerator, hot heat exchanger and the short section of 110 mm diameter thermal buffer tube are enclosed within a ceramic insulation material (DURATEC), with a thickness of 3.5 cm. The 110 mm diameter buffer tube connects to a smaller buffer tube via a short transition cone, which reduces the diameter from 110 mm to 54 mm over a distance of 20 mm. The small diameter buffer tube is around 100 mm long and has the internal diameter of 55 mm (a section of standard stainless steel 2 inch tube, with 2.77 mm wall thickness). Below the small diameter buffer tube, a secondary cold heat exchanger is introduced to prevent the hot air reaching the alternator housing. The secondary cold heat exchanger is made out of a piece of car radiator, which tightly fits inside the 2 inch pipe. A cooling water jacket is surrounding the outside of the pipe at this position.

The alternator housing is about 50 mm below the secondary cold heat exchanger. The alternator is mounted on the bottom flange of the housing; the cone facing downwards. The bottom flange has a small glass window (50 mm diameter), which is an optical access for the laser displacement sensor (MICROTRACK II) to measure the displacement of the alternator diaphragm. Two PCB pressure transducers (model 112A22, manufactured by PCB Piezoelectric) have been used to measure the pressures in front and behind the alternator diaphragm. They are marked as P1 and P2 in Figure 2.

The remaining part of the rig is the feedback tube, with the total length of 3.4 m. Because the engine is designed to operate with air at atmospheric pressure, the maximum pressure difference between the inside and the outside of the resonator corresponds to acoustic pressure, which is usually less than 0.1 bar. Therefore, the feedback pipe is made out of a standard 2 inch PVC pipe and 90° bends (Class E, OD: 60.3 mm, wall thickness 4.5 mm) instead of a metal pipe to reduce costs. The total length of the loop is 4.03 m. The measured frequency is 75 Hz. About 33 cm away from the alternator housing, a “stub” tube (a blind branch with an adjustable piston) is connected to the resonator to improve the impedance matching between the alternator and the engine. It has the same diameter as the feedback tube and is 37 cm long.

The loudspeaker (alternator) adopted in this work is B&C 6PS38 woofer manufactured by B&C Speakers [10]. Its specifications and the Thiele/Small parameters are summarized in Table 1. A high power variable resistor is adopted as an electrical load for the alternator to extract electrical power. The voltage difference and the current flowing through the load resistor are measured using a standard voltmeter and ammeter. As a result, the electrical power extracted by the load resistor can be deduced. The output from the sensors described together with the voltage drop V_L on the load resistor are recorded directly using a computer acquisition card (OMB-DAQTEM 14). The phase angles between these signals are measured by SR830 DSP lock-in amplifier.

Table 1. Specifications of the loudspeaker/alternator B&C 6PS38 [10].

Nominal Diameter	170 mm	Q_{ms}	11.7
F_s	75 Hz	S	132 cm^2
Bl	10.8 Tx/m	X_{max}	+/- 6 mm
L_e	0.6 mH	M_m	14 g
R_e	5.4 Ω	K_m	0.36 mm/N
Q_{es}	0.31	R_m	0.64 kg/s

4. Experimental results and discussion

With the terminals of the alternator open, the generator (i.e. the engine plus the alternator) starts to oscillate when the hot end temperature of the regenerator (T1) reaches 240 ºC. At this time, the cold end of the regenerator is at 30ºC, while the metal temperature of the hot heat exchanger is 291ºC. The onset temperature difference (T1-T4) is about 210 ºC. When the load resistor is connected to the alternator the onset temperature difference increases as the resistance decrease. For example, for 28.4 Ω load resistance the generator starts to oscillate when T1 reaches 261 ºC, the related onset temperature difference (T1-T4) being about 231 ºC. When the load resistance drops to zero (i.e. short circuit between the terminals), the onset temperature difference goes up to 500 ºC. All the experiments below are conducted for the generator in a steady state for selected levels of heat input.

4.1. Sample Measurement

As described above, the two pressure sensors P1 and P2 measure the pressure oscillations in front and behind the alternator diaphragm. The displacement sensor measures the motion of the diaphragm, which can be converted to its velocity. The phase angles between these oscillations can be either measured using a lock-in amplifier or by using FFT analysis of the simultaneously recorded signals. Combining these measurements, the acoustic power flow behind and in front of the alternator can be obtained, which gives the acoustic power absorbed by the alternator. Because the voltage drop on the resistor overflows the range of the computer acquisition card (+/- 10 V) at high power values, a case with relatively small V_L is selected for illustration. Figure 3 shows one sample of this type of measurement, for the input heat of 600 W, and the load resistor of 10.44 Ω.

Figure 3 shows five oscillations. Here, for the convenience of discussion, the displacement of the alternator diaphragm can be looked upon as a reference. It has amplitude of 2.64 mm. P1 and P2 are the pressure oscillations in

front and behind the alternator diaphragm. They have amplitudes of 2698 Pa and 1816 Pa, respectively. These two oscillations are almost in phase, but both lead the displacement. The measurement shows that P1 and P2 lead the displacement with a phase of 136º and 133º, respectively. It can also be seen that the voltage drop on the load resistor leads the displacement, and has amplitude of 6.66 V. The actual phase angle is measured as 91º. The volumetric velocity, U_1, is converted from the displacement sensor signal, which is 90º leading the displacement and has an amplitude 0.0164 m^3/s.

For further analysis, the results shown in Figure 3 can also be converted into a phasor diagram shown in Figure 4. It can be clearly seen that the pressure drop is around 127º, not $-\pi$, out of phase with velocity. This means that the alternator is off resonance. Using equations (3) – (5), the acoustic power flow to and from the alternator, and the acoustic power absorbed by the alternator can be obtained as 15.3 W, 10.9 W and 4.4 W respectively. The electrical power extracted by the load resistor is 2.12 W. Consequently, the obtained acoustic-electric conversion efficiency, $\eta_{A\text{-}E}$, is about 48%. This is relatively high for an off-the-shelf audio loudspeaker. However, the engine efficiency defined by the absorbed acoustic power over heat input, $\eta_{H\text{-}A}$, and the generator efficiency defined by the electrical power over heat input, $\eta_{H\text{-}E}$, are only 0.7% and 0.35%, respectively.

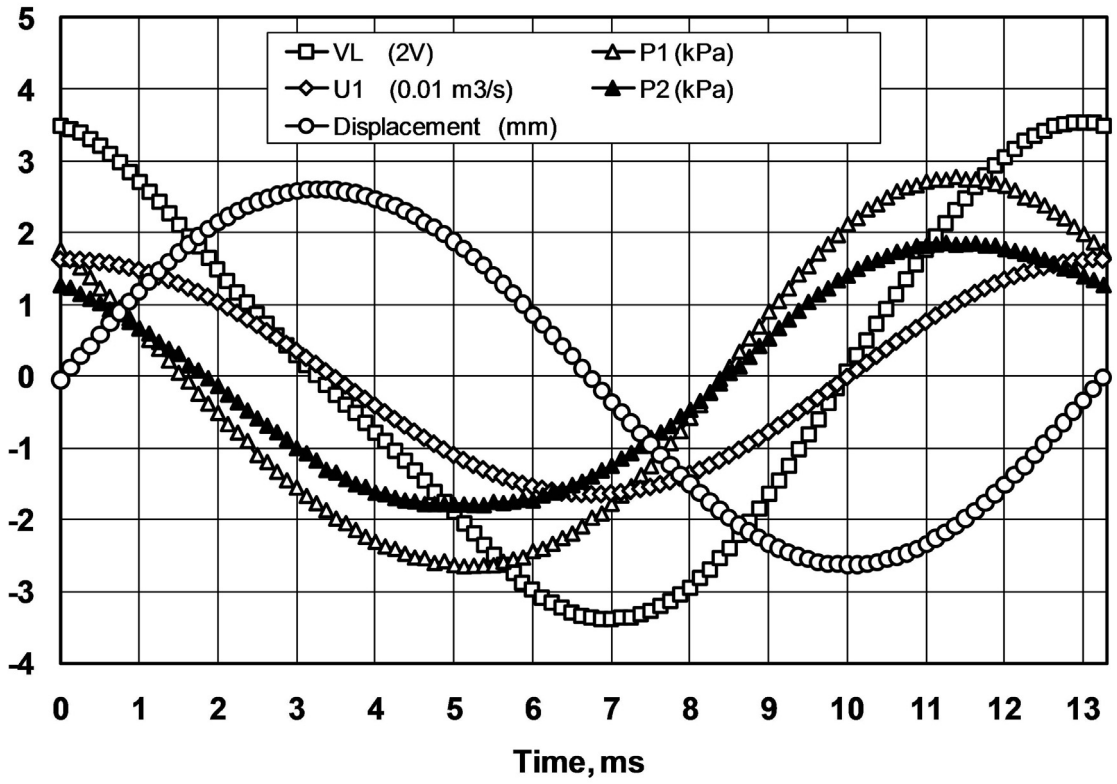

Figure 3 A sample measurement of alternator performance at heat input of 600 W and load resistance 10.44 Ω. Five curves are shown: pressure oscillations in front (P1) and behind (P2) of the alternator diaphragm, displacement of the diaphragm, voltage drop on the load resistor and calculated volumetric velocity.

4.2. Varying the input heat

Using the same measurement procedure, the generator performance can be tested by varying the input heat and the load resistance. This subsection shows the results obtained when the input heat varies from 300 to 800 W in 100 W steps, but the load resistance is fixed at 28.4 Ω. For each case, the measurement is conducted after the steady state is

reached. The results are shown in Figure 5. Here, the measured power is plotted against the temperature difference between the two ends of the regenerator (T1-T4). The triangles show the measured acoustic power transported from the thermoacoustic core to the alternator. The squares show the acoustic power absorbed by the alternator. The diamonds show the electrical power extracted by the load resistor. Interestingly, they all increases linearly with (T1-T4). The dashed line which is associated with the secondary axis on the right shows the dependence between the heat input and the generated temperature difference. For the input power of 800 W, the measured pressure amplitude is 5667 Pa at P3, which is around 5.6% of the mean pressure. The acoustic power that goes to the alternator is about 49.3 W, The acoustic power absorbed by the alternator is 10.3 W. The load resistor extracts 5.17 W of electrical power. Here, $\eta_{A\text{-}E}$ = 50%, $\eta_{H\text{-}A}$ = 1.29%, and $\eta_{H\text{-}E}$ = 0.65%.

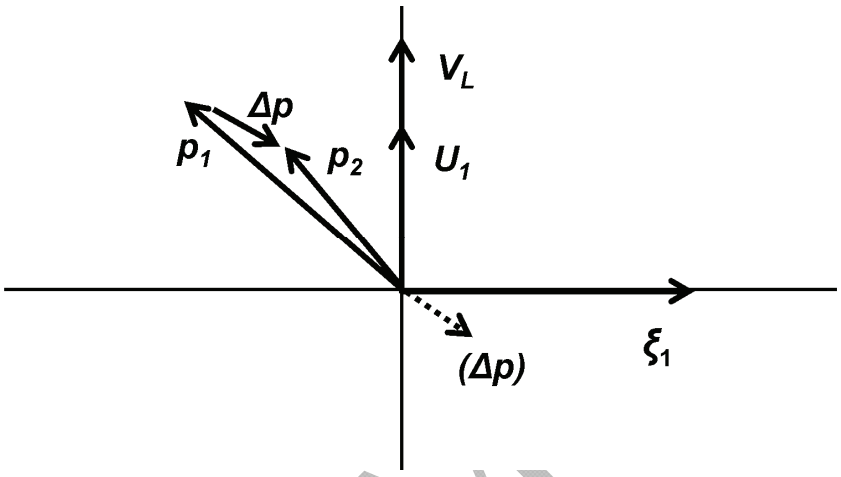

Figure 4 Phasor diagram related to the oscillations shown in Figure 3.

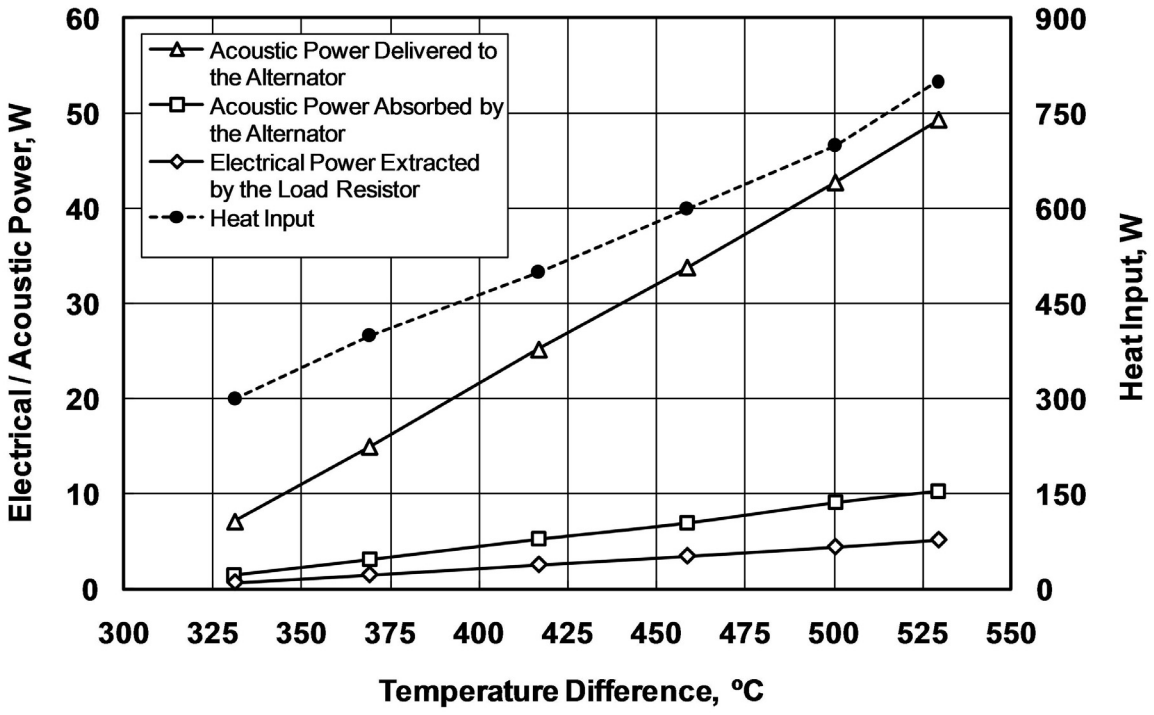

Figure 5 The measured powers (left vertical axis) versus the temperature difference between the two ends of the regenerator. Triangles show the measured acoustic power transported from the thermoacoustic core to the alternator. The squares show the acoustic power extracted by the alternator. The diamonds show the electrical power extracted by the load resistor. Dashed line with solid circles shows the dependence of the temperature difference on the value of heat input which can be read from the right vertical axis.

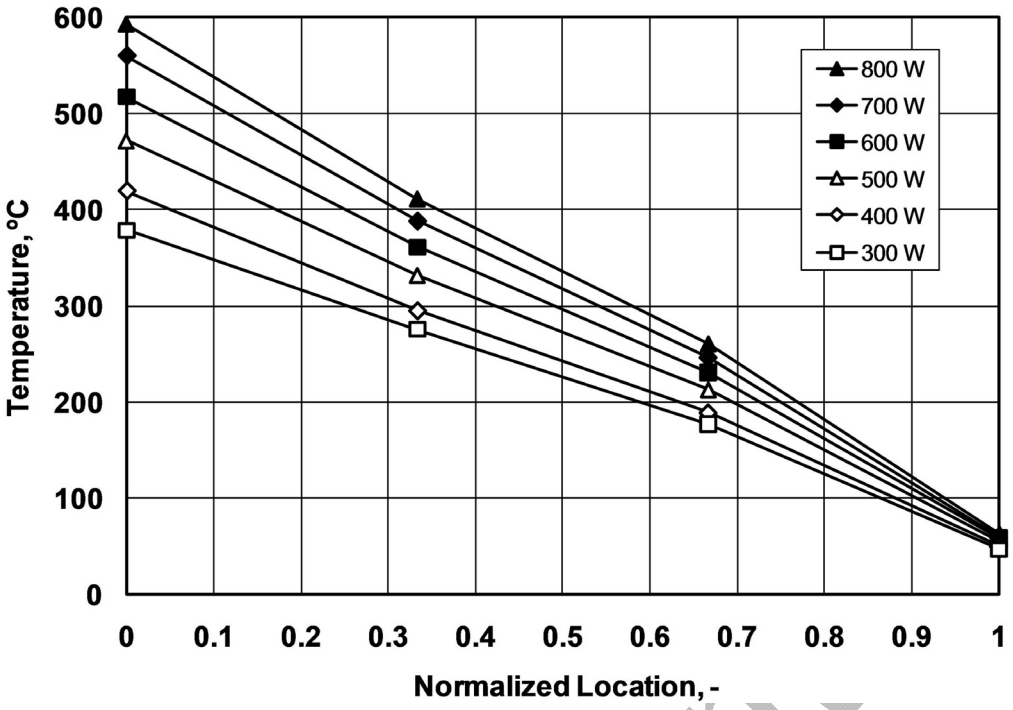

Figure 6 The temperature profiles along the regenerator for the cases studied in Figure 5.

For further analysis, the temperature profiles along the axis of the regenerator are plotted in Figure 6. The locations of the thermocouples are normalized by the regenerator length. It can be seen that the temperature profiles are not quite linear. As is well known, the temperature profile should be nearly linear in the absence of streaming within the regenerator. Therefore the temperature profiles in Figure 6 suggest that there is some acoustic streaming within the regenerator from hot end to the cold end. Of course, the diaphragm of the alternator separates the air on its two sides, which stops possible Gedeon streaming [2]. Therefore, there must be another reason for the nonlinear temperature profiles. The rig is mounted in such a way that the thermoacoustic core is vertical, with the regenerator above the hot heat exchanger. Therefore it is thought that natural convection is a possible reason for the nonlinear temperature profiles.

The above discussion indicates that the engine is very inefficient in converting heat to acoustic power. However Delta EC [11] simulations predict engine efficiencies as high as 5-6% (here the engine efficiency is understood as the ratio of acoustic power to heat input). Clearly, the engine still needs debugging and optimization. According to preliminary experiments, the heat loss is potentially an issue. To estimate the heat loss, two additional thermocouples are installed on the external surface of the ceramic insulation material and the 4 inch flange adjacent to the thermal buffer tube. For 800 W heat input, the metal temperature of the hot heat exchanger is 638 ºC. However, the surface temperature of the ceramic insulation is 304 ºC, and the surface temperature of the flange between the two thermal buffer tube sections is 196 ºC. These temperatures are relatively high and may explain high heat losses, although clearly calculating the heat losses precisely is not possible on the basis of the crude temperature measurements.

Furthermore, the impedance matching between the alternator and the engine needs more attention. As mentioned above, a “stub” is connected to the looped tube to improve impedance matching. Without the “stub”, the onset temperature difference is 40-50 ºC higher, and the extracted electrical power is 10-15% lower. The location and the length of the “stub” are selected experimentally to tune the acoustic impedance at the cold end of the regenerator to

nearly real. There is still some room for the optimization. Finally, at this stage, the alternator is installed next to the secondary cold heat exchanger. This location is a low impedance zone along the loop. In fact, almost a maximum alternator stroke is achieved for 800 W heat input. Therefore, if more electrical power is to be extracted, it should be installed at a high impedance zone to avoid the limitation of the alternator stroke.

4.3. Varying the load resistor

Following the already outlined experimental procedures, the generator was tested by varying the load resistance for three heat input values. Fig. 7 shows the measured electrical power extracted by the load resistor. It can be seen that when the heat input is fixed, there is an optimum load resistance which corresponds to the maximum electrical power that can be extracted. For example, for 600 W heat input, the optimum load resistance is about 31 Ω. Furthermore, the optimum load resistance depends on the level of heat input. It can be seen that for 700 W and 800 W heat input, the optimum load resistance is 26 Ω and 23 Ω, respectively. By inspecting equation (7), one can see that the extracted electrical power depends on both $|U_1|$ and R_L when the alternator is given. If $|U_1|$ is fixed, in order to extract more electrical power R_L should approach R_e. So reducing R_L from a very high value (for example 45 Ω in Figure 7) can increase the extracted electrical power. This can explain the tendency of the right branches of the curves in Figure 7.

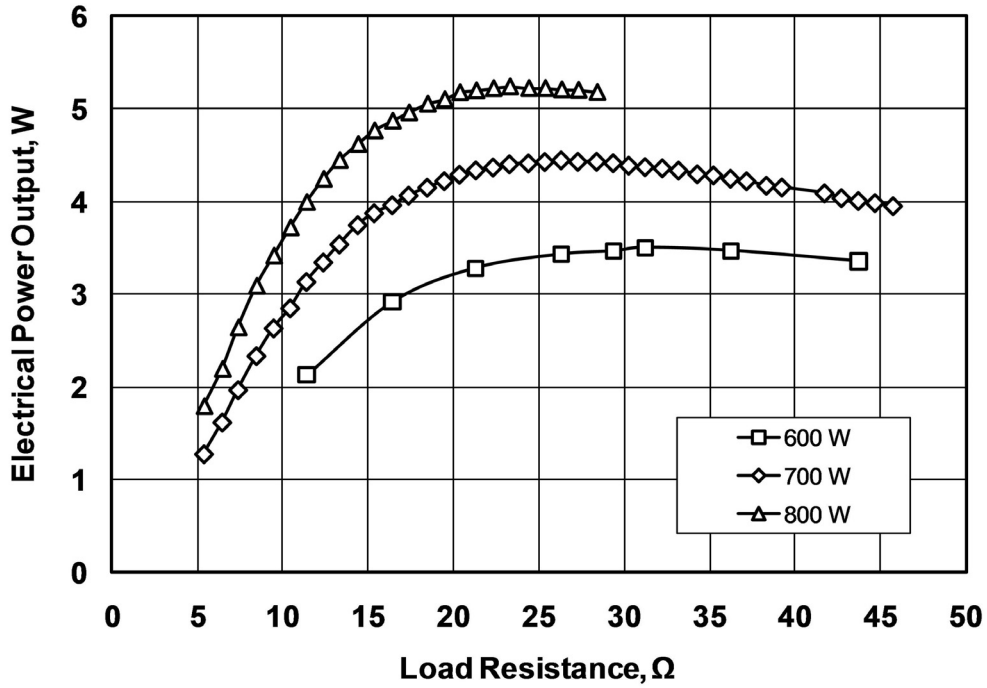

Figure 7 Measured electrical power as a function of the applied load resistance. Three curves for three different values of electrical heater power are plotted.

However, according to equation (13), as the load resistance decreases further, the equivalent acoustic impedance of the alternator increases quickly, and therefore, the interaction between the alternator and the engine becomes stronger. As a result, high pressure amplitude is required to drive the alternator. However, as the heat input is fixed, the possible pressure amplitude is also limited. Consequently, this high impedance dramatically decreases $|U_1|$. Therefore, the acoustic power flow through the alternator diaphragm, which is feeding back to the cold end of the regenerator, also decreases. Therefore, less net acoustic power can be produced in the regenerator. This is the reason for a sharp drop in the extracted electrical power when the load resistance decreases and approaches to R_e.

Figure 8 shows some further information about the impact of the load resistance on the alternator acoustic-electric efficiency. In Fig. 8 the input heat is fixed at 700 W. The square symbols are the measurement results, while the solid line is the efficiency calculated using equation (10) and parameters in Table 1. However it should be noted that, the parameters in Table 1 are provided by the manufacturer and are average values for this product. Therefore, the calculations in Fig. 8 are very approximate. For more accurate calculations, the alternator parameters need to be accurately measured. Nevertheless, Fig. 8 shows similar trends between experiments and analytical predictions. Furthermore, somewhat surprisingly, at low load resistance, the measured results are very close to the calculated ones. As the load resistance increases, the discrepancy becomes bigger. This trend can possibly be attributed to the increase of the displacement of the diaphragm. The experimental results show that the displacement amplitude increases from 1.96 mm to 5.1mm, when the load resistance increases from 5Ω to 40Ω. For this alternator, the maximum stroke is 6 mm. Therefore, the loss due to nonlinear effects becomes stronger when the diaphragm displacement approaches the maximum, and this will most likely decrease the acoustic-electric efficiency.

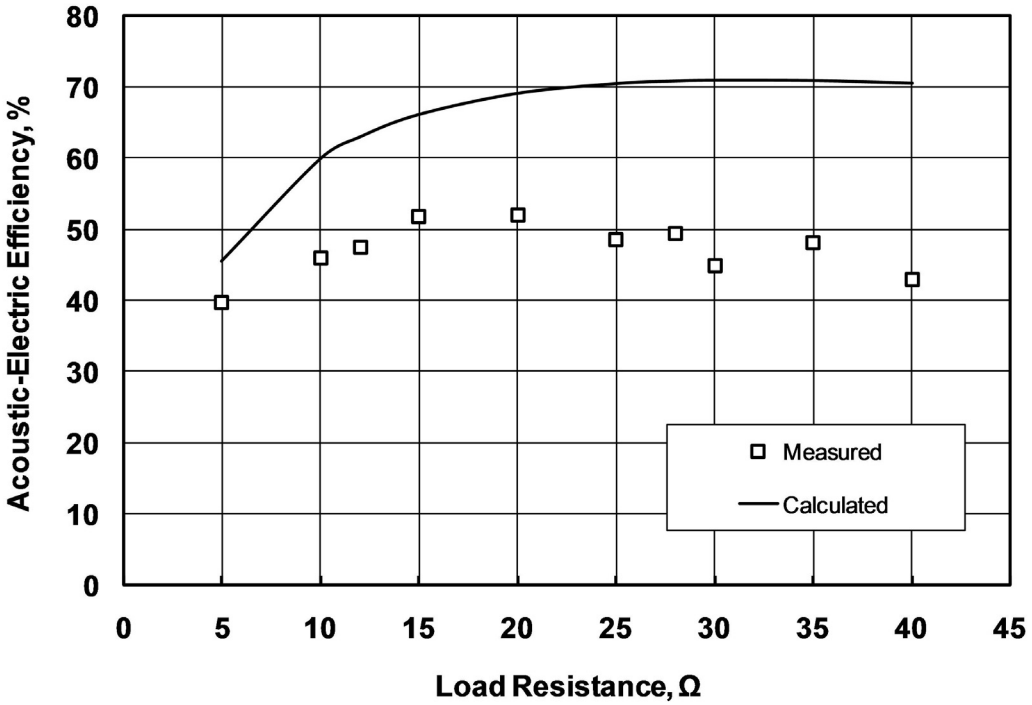

Figure 8 The acoustic-electric conversion efficiency of the alternator when the input heat is 700 W. The solid line is calculated using equation (10). The square symbols are the measured efficiencies when the load resistance varies.

5. Conclusions and future work

This paper describes the construction and experimental investigation of a thermoacoustic electricity generator, which uses the looped-tube travelling engine to convert thermal energy to acoustic power and a commercially available loudspeaker as an alternator, to convert the acoustic power to electricity. The device described is intended as a demonstration of a low-cost concept that could be further developed for rural and remote communities in developing countries. In this preliminary work, the alternator produced 5.17 W of electricity at an acoustic-electric conversion efficiency of 50%, at the heat input of 800 W. The results show that it is possible and feasible to use commercially available, low-cost loudspeakers to develop low-cost electrical generators based on thermoacoustic technologies. Furthermore, the tests of the alternator indicate that the simple linear model is still useful to describe its behaviour.

However, these preliminary results also show that, compared with Delta EC predictions, the engine efficiency is very low; as a result, the total generator efficiency is also very low (for example 5.17 W electrical output over 800 W heat input gives a figure of only 0.65%). Of course the considerable heat loss is likely to skew the overall performance figures unfavourably. Unfortunately, it is not possible to measure the exact split of the 800 W input between the actual heat going into the engine and lost to the environment, but preliminary estimates based on thermocouple measurements show that the loss to the surroundings may be as high as 40 or 50%, in which case the overall generator efficiency could be revised upwards to above 1%.

While the initial results are encouraging, it should also be noted that extensive re-engineering of the demonstrator is required in order to improve its performance. This of course will include a substantial change in the engine configuration to limit the heat loss. However, it will also be necessary to investigate the impedance matching between the alternator and the engine and the location of the alternator. Further work may also need to include the introduction of appropriate hot heat exchangers demonstrating the viability of a combustion driven heat input. All of these aspects will be addressed as future work.

Acknowledgement

The authors would like to acknowledge the support received from the Engineering and Physical Sciences Research Council (EPSRC) UK under grants EP/E044379/1 (SCORE), GR/T04502/01 (EPSRC Advanced Research Fellowship) and GR/T04519/01. Other members of the SCORE project are acknowledged for their comments on the manuscript.

List of Symbols

Bl	force factor of the alternator
F	force
F_s	resonance frequency
I_1	current
K_m	mechanical stiffness
L_e	inductance of coil
M_m	total mass of the diaphragm and the coil
p	pressure oscillation
P_a	acoustic power
P_e	electrical power
Δp	pressure drop through the diaphragm of the alternator
Q_{es}	electrical quality factor
Q_{ms}	mechanical quality factor
R_e	resistance of coil
R_L	load resistor
R_m	mechanical resistance
S	effective area of the alternator
U_1	volumetric velocity
u_1	velocity of the diaphragm
V_L	voltage on the resistor
X_{max}	maximum displacement of alternator

Z acoustic impedance

$\eta_{A\text{-}E}$ acoustic-electric conversion efficiency

$\eta_{H\text{-}A}$ engine efficiency

$\eta_{H\text{-}E}$ generator efficiency

θ phase angle between Δp and U_1

ω angular frequency

List of References

[1] Swift GW 1992 Analysis and Performance of a Large Thermoacoustic Engine, *J. Acous Soc. Am.*, **92** (3): 1551-1563

[2] Backhaus S and Swift GW 2000 A Thermoacoustic-Stirling Heat Engine: Detailed study, *J. Acoust. Soc. Am.*, **107**: 3148-3166

[3] De Blok CM 2008 Low Operating Temperature Integral Thermoacoustic Devices for Solar Cooling and Waste Heat Recovery, *Proc. of Acoustics'08*, June 29-July 4 2008, Paris, France

[4] Wollan JJ, Swift GW, Backhaus S and Gardner DL 2002 Development of a Thermoacoustic Natural Gas Liquefier, *Proceedings of AIChE Meeting*, New Orleans LA

[5] Backhaus S, Tward E and Petach M 2004 Travelling-wave Thermoacoustic Electric Generator *Applied Physics Letters*, **85** (6): 1085-1087

[6] Riley PH and Johnson M 2008 Generating Electricity from Burning Wood Using Thermo-acoustics for Use in Developing Countries, *Proc. of Acoustics'08*, June 29-July 4 2008, Paris, France

[7] Riley PH, Saha C and Johnson CJ 2010 Functional and Cost Requirements for a Low-Cost, Electricity Generating Cooking Stove for Developing Countries, *Technology and Society Magazine IEEE* (in press)

[8] Jordan EJ *Loudspeakers*, London, Focal Press, 1963

[9] Swift GW *Thermoacoustics, a Unifying Perspective for Some Engine and Refrigerators*, Acoustical Society of America, New York, 2002

[10] B&C SPEAKERS, Data Sheet of 6PS38, URL: http://www.bcspeakers.com

[11] Ward WC and Swift GW 1994 Design environment for low-amplitude thermoacoustic engines, *J. Acoust. Soc. Am.*, **95** (6): 3671- 3672